A structure-function analysis of the left ventricle

Edward P. Snelling[1], Roger S. Seymour[2], J. E. F. Green[3], Leith C. R. Meyer[1,4], Andrea Fuller[1,4], Anna Haw[1], Duncan Mitchell[1,5], Anthony P. Farrell[6,7], Mary-Ann Costello[8], Adian Izwan[5], Margaret Badenhorst[9], Shane K. Maloney[1,5]

[1]Brain Function Research Group, School of Physiology, University of the Witwatersrand, Johannesburg, South Africa;
[2]School of Biological Sciences, University of Adelaide, Adelaide, South Australia, Australia;
[3]School of Mathematical Sciences, University of Adelaide, Adelaide, South Australia, Australia;
[4]Department of Paraclinical Sciences, University of Pretoria, Pretoria, South Africa;
[5]School of Anatomy, Physiology and Human Biology, University of Western Australia, Crawley, Western Australia, Australia;
[6]Department of Zoology, University of British Columbia, Vancouver, British Columbia, Canada;
[7]Faculty of Land and Food Systems, University of British Columbia, Vancouver, British Columbia, Canada;
[8]Central Animal Service, University of the Witwatersrand, Johannesburg, South Africa; and
[9]School of Physiology, University of the Witwatersrand, Johannesburg, South Africa

Abstract

This study presents a structure-function analysis of the mammalian left ventricle and examines the performance of the cardiac capillary network, mitochondria, and myofibrils at rest and during simulated heavy exercise. Left ventricular external mechanical work rate was calculated from cardiac output and systemic mean arterial blood pressure in resting sheep (*Ovis aries*; n = 4) and goats (*Capra hircus*; n = 4) under mild sedation, followed by perfusion-fixation of the left ventricle and quantification of the cardiac capillary-tissue geometry and cardiomyocyte ultrastructure. The investigation was then extended to heavy exercise by increasing cardiac work according to published hemodynamics of sheep and goats performing sustained treadmill exercise. Left ventricular work rate averaged 0.017 W/cm^3 of tissue at rest and was estimated to increase to ~0.060 W/cm^3 during heavy exercise. According to an oxygen transport model we applied to the left ventricular tissue, we predicted that oxygen consumption increases from 195 nmol $O_2 \cdot s^{-1} \cdot cm^{-3}$ of tissue at rest to ~600 nmol $O_2 \cdot s^{-1} \cdot cm^{-3}$ during heavy exercise, which is within 90% of the oxygen demand rate and consistent with work remaining predominantly aerobic. Mitochondria represent 21-22% of cardiomyocyte volume and consume oxygen at a rate of 1,150 nmol $O_2 \cdot s^{-1} \cdot cm^{-3}$ of mitochondria at rest and ~3,600 nmol $O_2 \cdot s^{-1} \cdot cm^{-3}$ during heavy exercise, which is within 80% of maximum in vitro rates and consistent with mitochondria operating near their functional limits. Myofibrils represent 65–66% of cardiomyocyte volume, and according to a Laplacian model of the left ventricular chamber, generate peak fiber tensions in the range of 50 to 70 kPa at rest and during heavy exercise, which is less than maximum tension of isolated cardiac tissue (120–140 kPa) and is explained by an apparent reserve capacity for tension development built into the left ventricle.

Keywords: capillary; heart; work; mitochondria; myofibril

NEW & NOTEWORTHY

Our model of oxygen transport through left ventricular cardiac tissue shows that oxygen demands are easily satisfied at rest, but only just satisfied during simulated heavy exercise. We also find that cardiac mitochondria likely operate close to their functional limits during

heavy exercise. However, the cardiac myofibrils retain a reserve capacity for tension development, which possibly protects the left ventricle from excessive force loads during health and compensates for impaired function during disease.

this study presents a structure-function analysis of the mammalian left ventricle and examines the relationships that exist between the cardiac capillary network, mitochondria, and myofibrils and the extent to which these components perform under the contrasting conditions experienced at rest compared with simulated heavy exercise. The mean external mechanical work rate of the left ventricle (W = J/s) can be estimated from the product of cardiac output (l/s) and systemic mean arterial blood pressure (kPa = J/l), plus the rate at which kinetic energy (W) is imparted to the blood (18, 51). Left ventricular work rate increases with exercise intensity because each of the factors that contribute to cardiac work increase with the metabolic and perfusion requirements of the body. For instance, heavy exercise elicits a 2- to 6-fold increase in cardiac output and a 1.2- to 1.7-fold increase in systemic mean arterial blood pressure in dogs, goats, ponies, and calves (70), sheep (32), cattle and horses (31), and humans (68). In addition, the kinetic energy associated with accelerating the blood increases from negligible levels at rest to as high as 10–25% of total left ventricular work during heavy exercise (11, 18).

Examination of the structure-function relationships that exist between the left ventricle's capillary network, mitochondria, and myofibrils advances our understanding of the mechanisms that support the increase in left ventricular work from rest to heavy exercise. Similar structure-function analyses on skeletal muscle show that oxygen supply satisfies oxygen demand during low-intensity exercise but that oxygen demand exceeds its supply and diffusion across the capillary network during high-intensity exercise, such that aerobic metabolism is supplemented by anaerobic metabolism and lactate production (12, 27, 33, 70). Apparently, the volume density of capillaries and mitochondria in skeletal muscle reflects the muscle's aerobic metabolic capacity, not the muscle's total metabolic capacity (74). Structure-function analyses have also shown that as skeletal muscle work increases to its aerobic metabolic limits, mitochondrial respiration rates in vivo approach maximum rates measured in vitro, indicating that skeletal muscle mitochondria operate close to their functional capacity during maximum aerobic metabolic work (63). Structure-function analyses have also shown that locomotory exercise at preferred speeds in small mammals imposes peak stresses on the ankle extensors that are approximately one-third of the maximum isometric stress recorded in situ during artificial stimulation but that this reserve capacity for myofibril tension development is likely reduced during locomotion at maximum speeds (53). Application of similar structure-function analyses on the capillary network, mitochondria, and myofibrils of cardiac tissue will help identify key design features that allow the left ventricle to operate continuously and over the wide range of work rates experienced under normal operation.

Seeking to identify those key design features, we present a structure-function analysis of the left ventricular cardiac tissue system of sheep and goats. We took measurements of stroke volume, heart rate, cardiac output, and systemic arterial blood pressure in animals under mild sedation to estimate the left ventricular work rate at rest. Using the hearts on which the resting hemodynamic measures were made, we then perfused-fixed the left ventricle, imaged the cardiac tissue with transmission electron microscopy, and undertook a stereological quantification of the left ventricle's capillary-tissue geometry and cardiomyocyte ultrastructure. We then extended the investigation to include an analysis of the left ventricle during simulated heavy exercise by applying our structural data and increasing left ventricular work according to published hemodynamic data of sheep and goats performing sustained treadmill exercise.

MATERIALS AND METHODS

Animals.

All procedures were approved by the Animal Ethics Committees of the University of the Witwatersrand (2013/25/2B) and the University of Western Australia (RA/3/100/1241). Adult sheep, *Ovis aries* (3 males, 1 female), and adult goats, *Capra hircus* (2 males, 2 females), purchased from farm stock, were housed in large indoor enclosures, under a controlled temperature [23 ± 1°C (SD)] and lighting regime (12:12-h day-night) at the Central Animal Service of the University of the Witwatersrand, South Africa (~1,750-m elevation). Animals were transferred to the facility 8 wk before experimentation and trained to sit quietly in sternal recumbency while being handled by technicians. Animals were fed daily on a mix of cereals, vegetables, and commercial pellet, and water was provided ad libitum. Animal health was assessed daily, and body mass was recorded weekly to the nearest 0.05 kg (YH-T3; Associated Scale, Johannesburg, South Africa). All animals were fasted 12–24 h prior to measurements.

Hemodynamics and work of the left ventricle.

Physiological measurements were conducted in a controlled environment (23 ± 1°C) in a dedicated large-animal procedure room. To determine the left ventricular work rate at rest, each animal was mildly sedated with midazolam [0.3 mg/kg im (67); Dormicum; Roche Products, Johannesburg, South Africa] and was in a state that in human medicine would be called "conscious sedation." Individuals exhibited intact corneal reflex and partial loss of muscle tone and were nonresponsive to innocuous stimuli. The skin and underlying tissue of the left midneck region was locally anesthetized with lidocaine (5 ml sc; Lignocaine Hydrochloride Fresenius 2%; Fresenius Kabi, Midrand, South Africa) before a fluid-filled, cardiac output Swan-Ganz thermodilution catheter (2.3-mm outside diameter; 139HF75P; Edwards Lifesciences, Centurion, South Africa) was introduced into the left jugular vein. The port at the distal tip of the Swan-Ganz catheter was connected via a fluid-filled line to a precalibrated pressure transducer (Deltran II DPT-200; Utah Medical Products, Midvale, UT), which allowed real-time monitoring of blood pressure waveforms at the catheter tip. The Swan-Ganz catheter was advanced from the jugular vein through the cranial vena cava, right atrium, and right ventricle and into the pulmonary artery. We also catheterized an auricular artery in each animal with an intravenous catheter (0.7-mm outside diameter; Introcan; B. Braun, Melsungen, Germany) connected via a fluid-filled line to another precalibrated pressure transducer (Deltran II DPT-200), which provided continuous measurement of systemic arterial blood pressure. The pressure transducers were placed at the level of the scapulohumeral joint (level with the base of the heart) and connected via blood pressure amplifiers (FE117; ADInstruments, Sydney, NSW, Australia) to a data acquisition system (PowerLab; ADInstruments), which captured and displayed real-time hemodynamic information through data analysis software (LabChart 5; ADInstruments). The Swan-Ganz catheter's heating coil lay in the right ventricle, and a thermistor at the catheter tip lay in the pulmonary artery, allowing measurement of cardiac output through thermodilution principles. Once all equipment was in place, the animal was given 30–60 min to acclimate and for the cardiovascular system to stabilize, after which we measured cardiac output (l/s), systemic arterial blood pressure (kPa = J/l), heart rate (beats/s), and stroke volume (liters) for ~30 min.

The mean external mechanical work rate of the left ventricle ($\dot{E}_{lv}$; W = J/s) at rest was calculated according to the equation $\dot{E}_{lv} = \dot{Q}\bar{P}_b + \dot{E}_k$, where $\dot{Q}$ is cardiac output (l/s), $\bar{P}_b$ is systemic mean arterial blood pressure (kPa), and $\dot{E}_k$ is the rate at which kinetic energy (W) is transferred to the blood. Kinetic energy was quantified according to the equation $\dot{E}_k = (1/2)\dot{m}_b\bar{v}_{b(a)}^2$, where $\dot{m}_b$ is blood mass pumped over time (kg/s) and $\bar{v}_{b(a)}$ is mean aortic blood

velocity (m/s). In this equation, $\dot{m}_b$ is the product of cardiac output (l/s) and blood density (1.06 kg/l), and $\bar{v}_{b(a)}$ is the quotient of cardiac output and aorta luminal cross-sectional area (cm^2) (measured postmortem), divided by a factor of 10 for unit conversion. Absolute work rate was divided by body mass (kg) to obtain the body mass-specific left ventricular work rate (W/kg body mass). Absolute work rate was also divided by left ventricular tissue volume (cm^3) (measured postmortem) to obtain the volume-specific left ventricular work rate (W/cm^3 of tissue), which was then used to calculate volume-specific oxygen demand rate (nmol $O_2 \cdot s^{-1} \cdot cm^{-3}$ of tissue), assuming 4.50×10^{-4} J/nmol O_2 [respiratory quotient = 0.76 (66)] and a 20% external mechanical efficiency (37, 61, 76). To supplement our measurements on resting animals, we simulated heavy exercise by increasing the work rate and oxygen demand rate of the left ventricle by a factor of 3.5-fold, which we calculated from the factorial increase in cardiac output and systemic mean arterial blood pressure of sheep (adults, 28-kg mean body mass) and goats (adults, 30-kg mean body mass) obtained at rest and during sustained treadmill exercise (32, 33). This approach is supported by the reasonable agreement (within 16%) between the resting left ventricular work rates measured in the present study compared with the treadmill studies. Last, we consider the effect of a 15–25% range in external mechanical efficiency and the effect of a 2.5- to 4.5-fold increase in the oxygen demand rate of the left ventricle.

Chemical fixation of the left ventricle.

Once the physiological measurements were complete, each animal was given a lethal dose of pentobarbital (200 mg/kg iv; Euthapent; Kyron Laboratories, Johannesburg, South Africa). The thoracic cavity was opened, and the ascending aorta was cannulated in a retrograde direction so that the cannula tip lay immediately above the entrance to the coronary arteries. The coronary vascular system first was perfused with Ringer's solution containing lidocaine (0.5 mg/ml) and heparin (20 IU/ml) to clear blood from the vessels, followed by a fixative solution of 2.5% glutaraldehyde and 1.5% paraformaldehyde in 0.13 M phosphate + 0.02 M sucrose buffer (320 mosmol/kgH_2O, pH 7.4). Physiological perfusion pressures were generated by elevating the perfusate 1.5 m above the level of the heart, and an incision through the right atrial wall allowed perfusate to drain. A fine transmural strip of cardiac tissue was excised from two random locations through the left ventricular wall, and while immersed under a shallow layer of the fixative solution, each strip was cut into numerous ~1-mm^3 tissue blocks. One tissue block was sampled randomly from each of the two strips and processed through the remainder of the protocol. We made no attempt to fix the heart in a particular state of contraction, nor did we avoid sampling any particular region of the left ventricular wall. Each sample was immersed in the fixative solution for 12–36 h and then given buffer rinses (6 × 10 min) followed by secondary fixation in a 2% solution of osmium tetroxide (3 h). Each sample was rinsed with distilled water (3 × 10 min) and dehydrated progressively in 50, 60, 70, and 80% ethanol (10 min each) followed by immersions in 90% ethanol, 100% ethanol, and propylene oxide (2 × 10 min each). Samples then were infiltrated incrementally with an embedding resin (Araldite-Embed kit; Electron Microscopy Sciences, Hatfield, PA) at ratios of 3:1, 2:2, 1:3 (propylene oxide-resin) and then left overnight in pure resin. The following day, each sample was submerged with random orientation into individual embedding molds prefilled with pure resin and left to polymerize for 48 h in a 70°C oven.

Morphometry of the left ventricle.

Hearts were trimmed of fat and major vessels, rinsed with an isotonic saline solution (0.90% wt/vol NaCl), and weighed to 1 g. The left ventricle, comprising free wall plus septum (35), was dissected free and also weighed to 1 g. Left ventricular tissue volume (V_{lv}; cm^3) was calculated as $V_{lv} = M_{lv}\rho^{-1}$, where M_{lv} is left ventricular mass (g) and ρ is the mass density of cardiac tissue [~1.06 g/cm^3 (73)]. Unbiased estimates of the left ventricle's capillary-tissue

geometry and cardiomyocyte ultrastructure were obtained from the fixed samples of cardiac tissue by generating isotropic uniform random images for stereological analysis (29, 48). A 70-nm ultrathin section was cut at a random distance and orientation into each sample using an 8-mm glass knife, a 2.4-mm diamond knife (Ultra 45°; Diatome, Nidau, Switzerland) and an ultramicrotome (EM UC6; Leica Microsystems, Wetzlar, Germany). Ultrathin sections were placed onto 3-mm copper mesh grids, stained with uranyl acetate (15 min) and lead citrate (10 min), and viewed with a 100-kV transmission electron microscope (Tecnai G2; FEI, Hillsboro, OR) coupled to an in-column digital camera (Veleta; Olympus, Tokyo, Japan). Moving systematically along the length and breadth of each section, 10 random images were captured of left ventricular tissue (×1,700), cardiomyocyte ultrastructure (×11,500), capillaries (×4,200), and mitochondria (×60,000) (Fig. 1).

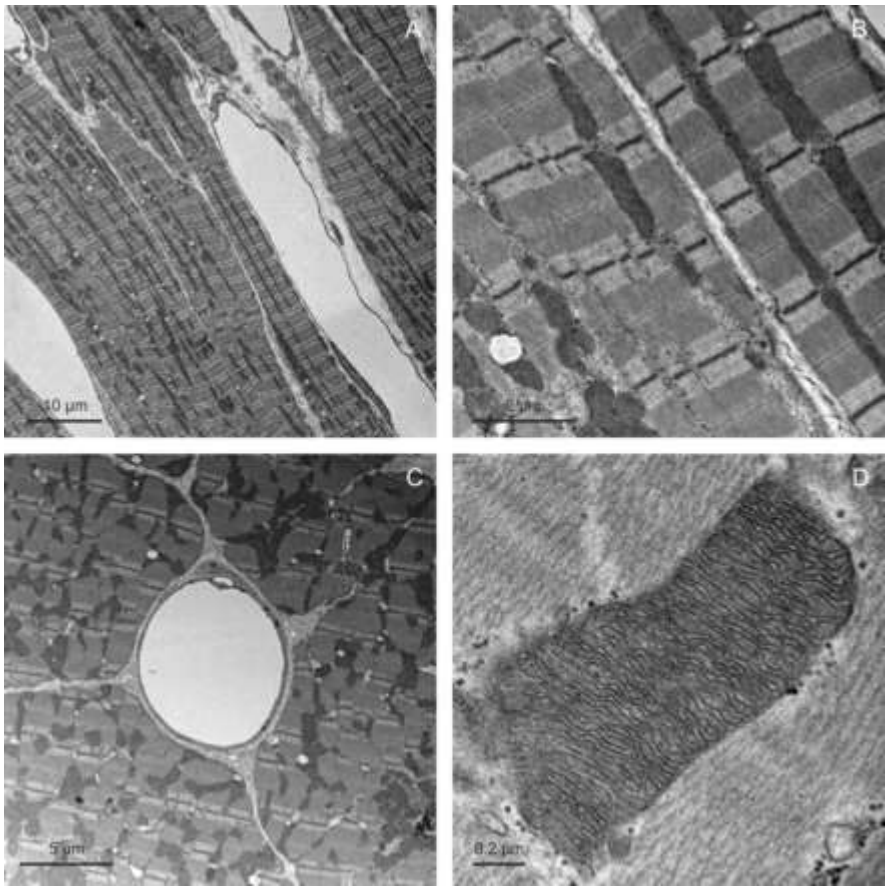

Fig. 1. Electron micrographs of left ventricular tissue showing the hierarchy of magnifications used for stereological analysis. *A*: low magnification (×1,700) used to determine the densities of cardiomyocytes, collagen, capillaries, fibroblast cells, pericytes, and other larger noncapillary vessels in the left ventricular tissue. *B*: high magnification (×11,500) used to determine the densities of myofibrils, mitochondria, sarcoplasmic reticuli, t-tubules, nuclei, and other components (cytosol, lipid, sarcolemma, intercalated disc) within the cardiomyocytes. *C*: capillary micrographs (×4,200) used for luminal diameter measurements. *D*: mitochondrion micrographs (×60,000) used for inner membrane surface density measurements. Images in *A*–*C* are from goats, and image in *D* is from a sheep.

Each image was imported into a computer graphics program (CorelDRAW 15; Corel, Ottawa, ON, Canada), where the images of left ventricular tissue were analyzed with a point grid test system superimposed randomly and the relative number of points falling on cardiomyocytes, fibroblast cells, pericytes, collagen, capillary lumen and endothelium, and other larger noncapillary vessels were counted. The total volume of each structure in the left ventricle (V_{str}; cm^3) was calculated as $V_{str} = V_{Vstr,lv}V_{lv}$, where $V_{Vstr,lv}$ is the fraction of left ventricular tissue occupied by the structure determined from the point grid counts (13, 46). Images of cardiomyocyte ultrastructure also were analyzed with a point grid test system

superimposed randomly, and the relative number of points hitting myofibrils, mitochondria, sarcoplasmic reticuli, t-tubules, nuclei, and other components (cytosol, lipid, sarcolemma, intercalated disc) were counted. Their respective volumes in the left ventricle (V_{org}; cm^3) were calculated as $V_{org} = V_{Vorg,card}V_{card}$, where $V_{Vorg,card}$ is the fraction of cardiomyocyte occupied by the organelle determined from the point grid counts and V_{card} is total left ventricular cardiomyocyte volume (cm^3). Images of mitochondria were analyzed with an isotropic Merz line test system superimposed randomly, and the surface area-to-volume ratio of the inner mitochondrial membrane ($S_{Vim,mito}$; cm^{-1}) was calculated as $S_{Vim,mito} = 2I^{-1}$, where I is the number of intersections of the test lines with the inner mitochondrial membrane surface and l is the total length (cm) of test lines falling over the mitochondrion (13, 46). The total surface area of inner mitochondrial membrane (S_{im}; cm^2) within the left ventricle was calculated as $S_{im} = S_{Vim,mito}V_{mito}$, where V_{mito} is mitochondrial volume (cm^3). Last, we analyzed the capillary-tissue geometry (16, 44). Images of capillaries were used to directly measure the cross-sectional luminal radius (R_c; cm). The mean radius of the tissue surrounding and serviced by each capillary (R_t; cm) could then be calculated as $R_t = R_c(V_{lv}/V_c)^{0.5}$, where V_{lv}/V_c is the left ventricle's tissue-to-capillary volume ratio. Next, the mean number of capillary profiles per unit cross-sectional area of left ventricular tissue ($N_{Ac,lv}$; cm^{-2}) was calculated as $N_{Ac,lv} = \pi^{-1}R_t^{-2}$. The mean number of capillary profiles per unit cross-sectional area of left ventricular fiber ($N_{Ac,card}$; cm^{-2}) was also calculated, $N_{Ac,card} = \pi^{-1}R_c^{-2}(V_{card}/V_c)^{-1}$.

Three-dimensional model for oxygen transport through the tissue of the left ventricle.

Under resting conditions, oxygen demand by the left ventricular cardiac tissue is equal to consumption, since supply is normally not limiting. To explore the possibility that oxygen supply could limit consumption when demand by the cardiac tissue is augmented during heavy exercise, we applied the dimensions of the left ventricle's capillary-tissue network and the oxygen demand rate of the left ventricular tissue during simulated heavy exercise to a three-dimensional model for oxygen transport through the capillaries and surrounding tissue. We considered a cylindrical capillary, surrounded by a cylindrical region of tissue. Our model is essentially a progression of the well-known Krogh cylinder model and Krogh-Erlang solution (39), which we adapted from McGuire and Secomb (47), incorporating the following features: decline in oxygen content of blood along the capillary path, intravascular resistance to oxygen transfer, myoglobin-facilitated diffusion, and Michaelis-Menten consumption kinetics. Failing to incorporate these features into the Krogh cylinder model has previously been discussed (38) and analyzed (19). Nonetheless, our model requires a number of simplifying assumptions, including the following: capillaries are straight and parallel, of constant radius and length, and homogeneously distributed; capillary blood flow is unidirectional and constant, and its velocity across the capillary cross section is invariant; oxygen content of blood entering the capillary is invariant; oxygen content of blood across the capillary cross section is also invariant, and oxygen and hemoglobin are in chemical equilibrium; oxygen flux into the tissue occurs only via the capillaries, where it is cylindrically symmetrical, and does not proceed beyond the outer limit of the tissue cylinder; oxygen diffusion occurs only in the radial direction; oxygen transport does not occur by convective mixing; oxygen consumption rate is homogeneous in the tissue; and the system is in steady state (17, 19, 38).

The input parameters for the oxygen transport model were averaged for sheep and goats, and values of constants were obtained from the literature (Table 1). Axial distance along the capillary path was denoted z (cm), and radial distance from the center of the capillary was denoted r (cm). Capillary path length was denoted L (cm) and was defined as the mean minimum path length from arteriole to venule. The oxygen partial pressure (Po_2) of the blood was denoted p_b (kPa). Noncapillary tissue occupies the region $R_c < r < R_t$, and the Po_2 in that tissue was denoted p_t (kPa). Diffusion of oxygen through the tissue is assumed to occur

predominantly in the radial direction and is facilitated by myoglobin, which we accounted for by defining p_t* (kPa), the myoglobin-facilitated Po_2, to be

$$p_t^* = p_t + \frac{D_{mb} C_{mb} V_{mb}}{K_t} \left(\frac{p_t}{p_{50\ mb} + p_t} \right) \quad (1)$$

Table 1. Values used to model oxygen transport and Po_2 profiles through the capillaries and tissue of the left ventricle during simulated heavy exercise

	Parameter	Value	Units	Reference
$N_{Ac,lv}$	Capillary density (number per area of tissue)	239,600	cm^{-2}	This study
R_c	Capillary lumen radius	0.00036	cm	This study
R_t	Tissue cylinder radius	0.0012	cm	This study
L	Capillary path length[a]	0.060	cm	6, 7, 8, 9, 34
$V_{Vc,lv}$	Capillary lumen volume density	9.5	%	This study
$\dot{V}_{b(t)}$	Volume-specific tissue perfusion rate[b]	0.088	$cm^3 \cdot s^{-1} \cdot cm^{-3}$	15
$\bar{v}_{b(c)}$	Capillary mean blood velocity	0.056	cm/s	This study, 15
$\dot{V}o_{2(dem)}$	Volume-specific O_2 demand rate[c]	670	$nmol \cdot s^{-1} \cdot cm^{-3}$	This study, 32, 33
p_{50hb}	Po_2 of Hb half-max saturation[h, i]	4.1	kPa	41
p_{50mb}	Po_2 of Mb half-max saturation[h, i]	0.34	kPa	59, 60
p_{50cyt}	Po_2 of cytochrome oxidase half-max saturation[i]	0.050	kPa	58, 77
$p_{b(i)}$	Po_2 of blood at the capillary entrance (z = 0)[d]	16.6	kPa	10, 70
C_b	Blood O_2 carrying capacity[e]	7,170	$nmol/cm^3$	14, 33, 49
K_t	Krogh diffusion constant for cardiac tissue[f, h]	3.8×10^{-9}	$cm^2 \cdot s^{-1} \cdot kPa^{-1}$	72
K_{pl}	Krogh diffusion constant for plasma[h]	5.2×10^{-9}	$cm^2 \cdot s^{-1} \cdot kPa^{-1}$	69
D_{mb}	Mb diffusion coefficient for cardiac tissue[f, h]	5.0×10^{-7}	cm^2/s	20, 42, 52
C_{mb}	Mb concentration of cardiac tissue[g]	219	$nmol/cm^3$	50
V_{mb}	Mb molar volume	2.2×10^{-5}	$cm^3/nmol$	47
Sh_c	Sherwood number	2.5	–	22
n	Hill's n value	2.7	–	56

Averaged sheep and goat values are given unless stated otherwise.

Hb, hemoglobin; Mb, myoglobin; max, maximum.
[a] Mean minimum path length from arteriole to venule, averaged from cardiac tissue across various mammal species;
[b] averaged cardiac tissue perfusion rates across various mammal species during heavy exercise;
[c] calculated from the left ventricular hemodynamic scope of sheep and goats during heavy exercise, see materials and methods;
[d] mean value of arterial blood in sheep and goats during heavy exercise, assuming negligible precapillary oxygen losses under conditions of high oxygen use;
[e] calculated according to the blood hemoglobin concentration of sheep and goats during heavy exercise, and a functional oxygen-hemoglobin binding capacity of 60,290 nmol O_2/g;
[f] derived from rat cardiac tissue;
[g] mean value across various mammal species.
[h] 37°C;
[i] pH 7.4.

where D_{mb} is the myoglobin diffusion coefficient (cm^2/s), C_{mb} is the concentration of myoglobin ($nmol/cm^3$), V_{mb} is the molar volume of myoglobin ($cm^3/nmol$), and p_{50mb} is the Po_2 at which myoglobin is half saturated (kPa). We assumed that oxygen diffuses within the tissue with a Krogh diffusion constant K_t ($cm^2 \cdot s^{-1} \cdot kPa^{-1}$), is used at a rate $\dot{V}o_2(p_t^*)$ (nmol $O_2 \cdot s^{-1} \cdot cm^{-3}$ of tissue), and hence varies with position in the tissue dependent on p_t*. The

governing equation for oxygen transport in the tissue is thus

$$\frac{K_t}{r}\frac{\partial}{\partial r}\left(r\frac{\partial p_t^*}{\partial r}\right) = \dot{V}\,O_2(p_t^*) = \frac{\dot{V}\,O_2(\,dem\,)^{p_t^*}}{p\,50\;\;cyt\;\;+p_t^*}H(p_t^*) \quad (2a)$$

where $\dot{V}o_{2(dem)}$ is the oxygen demand rate of cardiac tissue during heavy exercise (nmol $O_2 \cdot s^{-1} \cdot cm^{-3}$ of tissue) and p_{50cyt} is the Po_2 at which oxygen consumption is half the maximal value (kPa). The Heaviside function, $H(p_t^*)$ [where $H(p_t^*) = 1$ if $p_t^* > 0$, and 0 otherwise], is included to permit oxygen consumption only when there is a positive Po_2. This equation was solved subject to two boundary conditions: one at the capillary wall, $r = R_c$, and the other at the outer limit of the tissue cylinder, $r = R_t$. At the capillary wall, the flux of oxygen into the tissue is assumed to be proportional to the difference in Po_2 across the wall, i.e.,

$$2\pi R_c K_t \frac{\partial p_t^*}{\partial r} = -T_c(p_b - p_t) \quad \text{on } r = R_c \quad (2b)$$

where T_c is the capillary mass transfer coefficient ($cm^2 \cdot s^{-1} \cdot kPa^{-1}$), which is equal to $\pi K_{pl} Sh_c$, where K_{pl} is the Krogh diffusion constant for plasma ($cm^2 \cdot s^{-1} \cdot kPa^{-1}$) and Sh_c is the Sherwood number. By the symmetry of the assumed geometry, there is no oxygen flux out of the tissue cylinder at $r = R_t$, and we thus imposed

$$\left(\frac{\partial p_t^*}{\partial r}\right) = 0 \text{ on } r = R_t \quad (2c)$$

We also required an equation to describe the Po_2 of the blood flowing down the capillary. As oxygen is consumed by the surrounding tissue, so p_b will decrease with distance along the capillary. We assumed the oxygen content of the blood, C (nmol/cm^3), is related to p_b by

$$C = C_b S_{hb}(p_b) = C_b \frac{\left(p_b/p_{50\,hb}\right)^n}{1 + \left(p_b/p_{50\,hb}\right)^n} \quad (3)$$

where C_b is the oxygen carrying capacity of the blood (nmol/cm^3), p_{50hb} is the Po_2 at which hemoglobin is half saturated (kPa), and Hill's n value defines the degree of cooperativity. We further assumed that p_b is independent of r and that blood flow occurs with a velocity $\bar{v}_{b(c)}$ (cm/s) that is constant across the capillary. Assuming a steady state has been reached, conservation of mass implies

$$\dot{V}_{b(c)}\left(\frac{\partial C}{\partial z}\right) = -T_c(p_b - p_t) \quad (4a)$$

where $\dot{V}_{b(c)}$ represents blood flux down the capillary (cm^3/s) and is equal to $\pi R_c^2 \bar{v}_{b(c)}$ and $\pi R_c^2 L(\dot{V}_{b(t)}/V_{Vc,lv})$, where $\dot{V}_{b(t)}$ is cardiac tissue perfusion rate ($cm^3 \cdot s^{-1} \cdot cm^{-3}$) and $V_{Vc,lv}$ is capillary lumen volume density expressed as a fraction. *Equation 4a* was solved subject to the boundary condition

$$C = C(p_{b(i)}) \quad \text{at } z = 0 \quad (4b)$$

where $p_{b(i)}$ (kPa) is the initial value of p_b at $z = 0$, i.e., the Po_2 of blood as it enters the capillary.

We also calculated the oxygen consumption rate of cardiac tissue during heavy exercise, $\dot{V}o_{2(con)}$ (nmol $O_2 \cdot s^{-1} \cdot cm^{-3}$ of tissue). At steady state, the total oxygen consumed by the tissue per unit time must equal the oxygen flux into it. Thus, using *Eq. 2b*, we have

$$\dot{V}\,O_{2(\,con\,)} = \frac{1}{\pi(R_t^2 - R_c^2)L}\int_0^L T_c[p_b(z) - p_t(R_c, z)]\,dz \quad (5)$$

Statistical and modeling analyses.

All mean values are presented with 95% confidence intervals (CI) unless stated otherwise. Statistical significance between means was set at 0.05 a priori and tested using paired or unpaired two-tailed *t*-tests, for equal or unequal variance, as appropriate (78). Statistical tests were performed with data analysis software (Prism 6; GraphPad Software, La Jolla, CA). Simulations of the oxygen transport model were run with mathematical software (MATLAB R2013a; MathWorks, Natick, MA). Solutions for the governing equations, *Eqs. 2a–2c*, *3*, *4a*, and *4b*, were computed using an N*z* × N*r* grid (120 × 80).

RESULTS

Hemodynamics and work of the left ventricle.

Body mass, heart mass, and left ventricular mass were all significantly larger in sheep compared with goats (*t*-test, $P < 0.05$; Table 2). However, body mass-specific left ventricular mass was not significantly different between sheep and goats ($P > 0.05$), averaging 1.8 g/kg across all animals, which equates to 0.18% of body mass.

Table 2. Body mass, heart mass, left ventricular mass, and left ventricular mass of sheep and goats

	Sheep (*n* = 4)	Goat (*n* = 4)	*t*-Test
Body mass, kg	48 (±13)	28 (±6)	$t_6 = 2.9$, $P = 0.03$
Heart mass, g	139 ± 53	69 ± 7	$t_6 = 2.6$, $P = 0.04$
Left ventricular mass,* g	90 ± 30	46 ± 4	$t_6 = 2.9$, $P = 0.03$
Body mass-specific left ventricular mass,* g/kg	1.8 ± 0.2	1.7 ± 0.2	$t_6 = 0.93$, $P = 0.39$

Body mass values are means (±SD). Heart and left ventricular mass values are means ± 95% CI.
* Left ventricle defined as free wall plus septum.

At rest, the body mass-specific stroke volume was statistically indistinguishable between sheep and goats ($P > 0.05$; Table 3), averaging 0.0012 l/kg across all animals. Likewise, resting heart rate was not significantly different between sheep and goats ($P > 0.05$), with an overall mean of 1.7 beats/s. Resting cardiac output was statistically indistinguishable between sheep and goats ($P > 0.05$), averaging 0.076 l/s across all animals. Resting systemic mean arterial blood pressure was also statistically indistinguishable between sheep and goats ($P > 0.05$), with an overall mean of 14.5 kPa (= 109 mmHg).

Table 3. Left ventricular hemodynamics, volume-specific external mechanical work rate, and volume-specific oxygen demand rate of sheep and goats under resting conditions elicited by mild sedation

	Sheep (*n* = 4)	Goat (*n* = 4)	*t*-Test
Stroke volume, liters	0.053 ± 0.010	0.035 ± 0.003	$t_6 = 3.3$, $P = 0.02$
Body mass-specific stroke volume, l/kg	0.0011 ± 0.0003	0.0013 ± 0.0002	$t_6 = 0.91$, $P = 0.40$
Heart rate, beats/s	1.9 ± 0.6	1.4 ± 0.2	$t_6 = 1.6$, $P = 0.17$
Cardiac output, l/s	0.101 ± 0.042	0.051 ± 0.007	$t_6 = 2.3$, $P = 0.06$
Systemic mean arterial pressure,* kPa	16.2 ± 2.6	12.9 ± 0.9	$t_6 = 2.3$, $P = 0.06$
Mechanical work rate,† W/cm^3 of tissue	0.019	0.015	
O_2 demand rate,‡ nmol $O_2 \cdot s^{-1} \cdot cm^{-3}$ of tissue	220	170	

Values are means ± 95% CI.
* 1 kPa = 7.5 mmHg.
† Calculated as the product of cardiac output and systemic mean arterial blood pressure, plus the kinetic energy (W) associated with accelerating the blood.
‡ Calculated from work rate assuming 4.50×10^{-4} J/nmol O_2 and a 20% external mechanical efficiency.

At rest, the body mass-specific left ventricular work rate of the sheep and goats averaged 0.029 W/kg, and the volume-specific left ventricular work rate averaged 0.017 W/cm^3 of tissue, which corresponds to a mean volume-specific oxygen demand rate of 195 nmol $O_2 \cdot s^{-1} \cdot cm^{-3}$ (Table 3). During simulated heavy exercise, we calculated that the volume-specific left ventricular work rate would increase by ~3.5-fold to ~0.060 W/cm^3 of tissue, with a mean volume-specific oxygen demand rate of ~670 nmol $O_2 \cdot s^{-1} \cdot cm^{-3}$.

Morphometry of the left ventricle.

The body mass-specific volumes of the various components of the left ventricular tissue did not differ significantly between sheep and goats (*t*-test, $P > 0.05$; Table 4). Of the left ventricular tissue volume of sheep and goats, cardiomyocytes occupied 76–78%, the collagen framework occupied 6–7%, and the small fibroblast cells occupied 1%. The capillaries (lumen + endothelium) occupied most of the remainder of the tissue volume, 11–13%, with the lumen representing ~9.5%. Averaged across all animals, there were 239,600 capillaries/cm^2 of left ventricular tissue (= 2,396 mm^{-2}) or 315,100 capillaries/cm^2 of left ventricular fiber (= 3,151 mm^{-2}), the capillary lumen radius was 0.00036 cm (= 3.6 μm), and each capillary serviced a surrounding tissue cylinder with an average radius of 0.0012 cm (= 12 μm) (Table 5).

Table 4. Body mass-specific volume of left ventricular tissue components of sheep and goats

Body Mass-Specific Volume, cm^3/kg	Sheep (*n* = 4)	Goat (*n* = 4)	*t*-Test
Cardiomyocyte	1.4 ± 0.3	1.2 ± 0.2	$t_6 = 0.92$, $P = 0.39$
Collagen	0.11 ± 0.06	0.10 ± 0.04	$t_6 = 0.35$, $P = 0.74$
Capillary lumen	0.14 ± 0.06	0.17 ± 0.07	$t_6 = 0.56$, $P = 0.59$
Capillary endothelium	0.048 ± 0.014	0.032 ± 0.010	$t_6 = 1.8$, $P = 0.12$
Noncapillary vessels	0.044 ± 0.033	0.060 ± 0.045	$t_6 = 0.56$, $P = 0.60$
Fibroblast	0.016 ± 0.003	0.016 ± 0.010	$t_6 = 0.12$, $P = 0.91$
Pericyte	0.0042 ± 0.0040	0.0056 ± 0.0040	$t_6 = 0.48$, $P = 0.65$

Values are means ± 95% CI.

Table 5. Capillary-tissue network dimensions of the left ventricle of sheep and goats

	Sheep (*n* = 4)	Goat (*n* = 4)	*t*-Test
Capillary density (number per area of tissue),* cm^{-2}	223,100 ± 53,200	256,100 ± 106,600	$t_6 = 0.54$, $P = 0.61$
Capillary density (number per area of fiber),* cm^{-2}	292,200 ± 89,300	338,100 ± 143,100	$t_6 = 0.53$, $P = 0.61$
Capillary lumen radius,† cm	0.00034 ± 0.00006	0.00037 ± 0.00006	$t_6 = 0.77$, $P = 0.47$
Tissue cylinder radius,† cm	0.0012 ± 0.0002	0.0012 ± 0.0003	$t_6 = 0.26$, $P = 0.81$

Values are means ± 95% CI.
* 1 cm^{-2} = 0.01 mm^{-2}.
† 1 cm = 10,000 μm.

The body mass-specific volumes of the various organelles contained within the left ventricular cardiomyocytes also did not differ significantly between sheep and goats (*t*-test, $P > 0.05$; Table 6). Of the left ventricular cardiomyocyte volume of sheep and goats, myofibrils took up most of the space, occupying 65–66% of cardiomyocyte volume, followed by mitochondria, which occupied 21–22%. The sarcoplasmic reticulum network occupied 2.1–2.3% of cardiomyocyte volume, and the t-tubule system occupied 1.6–2.1%.

Table 6. Body mass-specific volume of left ventricular cardiomyocyte organelles and other components (cytosol, lipid, sarcolemma, intercalated disc) of sheep and goats

Body Mass-Specific Volume, cm^3/kg	Sheep (n = 4)	Goat (n = 4)	t-Test
Myofibril	0.88 ± 0.14	0.79 ± 0.10	t_6 = 0.96, P = 0.37
Mitochondria	0.31 ± 0.11	0.26 ± 0.03	t_6 = 0.93, P = 0.39
Sarcoplasmic reticulum	0.030 ± 0.020	0.028 ± 0.006	t_6 = 0.23, P = 0.82
t-Tubule	0.022 ± 0.010	0.024 ± 0.006	t_6 = 0.24, P = 0.82
Nucleus	0.016 ± 0.013	0.015 ± 0.020	t_6 = 0.10, P = 0.92
Other components	0.109 ± 0.045	0.088 ± 0.027	t_6 = 0.75, P = 0.48

Values are means ± 95% CI.

The inner mitochondrial membrane architecture did not differ significantly between sheep and goats (t-test, $P > 0.05$; Table 7). Averaged across all animals, the inner mitochondrial membrane surface density was 370,000 cm^2/cm^3 of mitochondria (= 37 m^2/cm^3), and the total body mass-specific inner mitochondrial membrane surface area was 104,000 cm^2/kg.

Table 7. Mitochondrial inner membrane surface dimensions of the left ventricle of sheep and goats

	Sheep (n = 4)	Goat (n = 4)	t-Test
Inner membrane surface density,* cm^2/cm^3 of mitochondria	355,000 ± 40,000	389,000 ± 29,000	t_6 = 1.35, P = 0.23
Inner membrane surface area, cm^2/kg	108,000 ± 27,800	100,000 ± 12,500	t_6 = 0.51, P = 0.63

Values are means ± 95% CI.
* 1 cm^2/cm^3 = 0.0001 m^2/cm^3.

Three-dimensional model for oxygen transport through the tissue of the left ventricle.

The oxygen transport model that we applied to the left ventricular tissue of sheep and goats predicted that during heavy exercise the average blood Po_2 would decrease along the length of the cardiac capillary, from 16.6 kPa at the arteriolar end to 0.6 kPa at the venular end. The Po_2 would also decrease radially through the tissue at all positions along the capillary-tissue cylinder. Nonetheless, almost all regions of the tissue would remain oxygenated, with just 9% of the tissue operating at $Po_2 < 0.05$ kPa and only 1.8% at $Po_2 < 0.01$ kPa (Fig. 2*A*). These percentages would of course vary over the probable range of the left ventricle's oxygen demand rate (Fig. 2*B*) and external mechanical efficiency (Fig. 2*C*). Assuming an intermediate efficiency of 20%, as the demand for oxygen increases to its calculated rate of ~670 nmol $O_2 \cdot s^{-1} \cdot cm^{-3}$ of tissue during heavy exercise, the consumption of oxygen increases in near unison, until it reaches a value of ~600 nmol $O_2 \cdot s^{-1} \cdot cm^{-3}$, which is just short of the estimated rate at which oxygen is delivered convectively in the blood, ~645 nmol $O_2 \cdot s^{-1} \cdot cm^{-3}$ (Fig. 3).

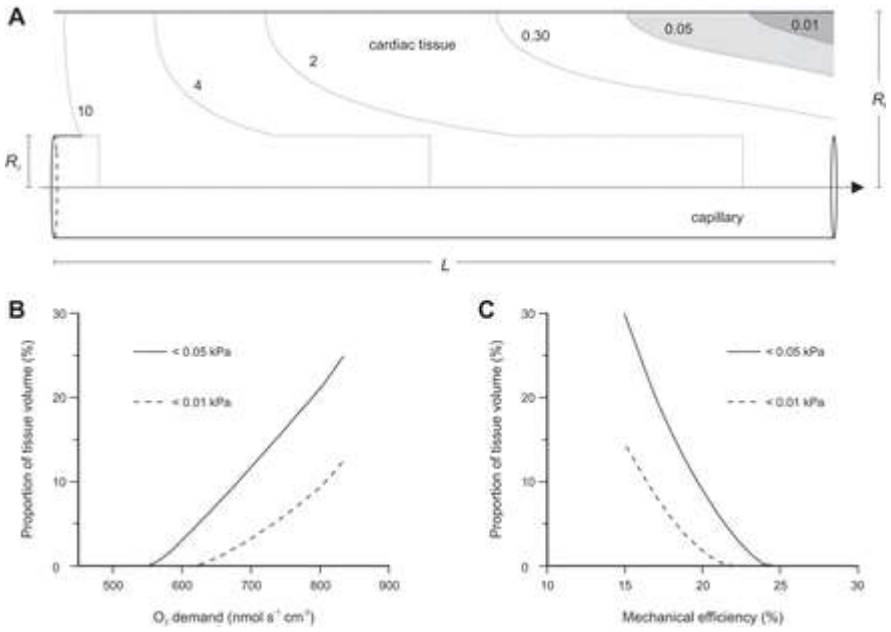

Fig. 2. Output of the oxygen transport model that we applied to the left ventricular tissue of sheep and goats during simulated heavy exercise. *A*: blood entering the capillary has a Po_2 of 16.6 kPa, whereas blood exiting has a Po_2 of 0.6 kPa. Tissue regions operating at Po_2 levels <0.05 kPa (light grey) and <0.01 kPa (dark grey) are shown. Mean capillary path length (L) is 0.060 cm, capillary radius (R_c) is 0.00036 cm, and tissue cylinder radius (R_t) is 0.0012 cm. This is for the standard case assuming an oxygen demand rate of 670 nmol $O_2 \cdot s^{-1} \cdot cm^{-3}$ of tissue and an external mechanical efficiency of 20%. *B*: predicted effect of varying the oxygen demand rate (nmol $O_2 \cdot s^{-1} \cdot cm^{-3}$ of tissue) on the proportion of cardiac tissue operating at Po_2 levels <0.05 and <0.01 kPa. *C*: predicted effect of varying the external mechanical efficiency (%) on the proportion of cardiac tissue operating at <0.05 and <0.01 kPa.

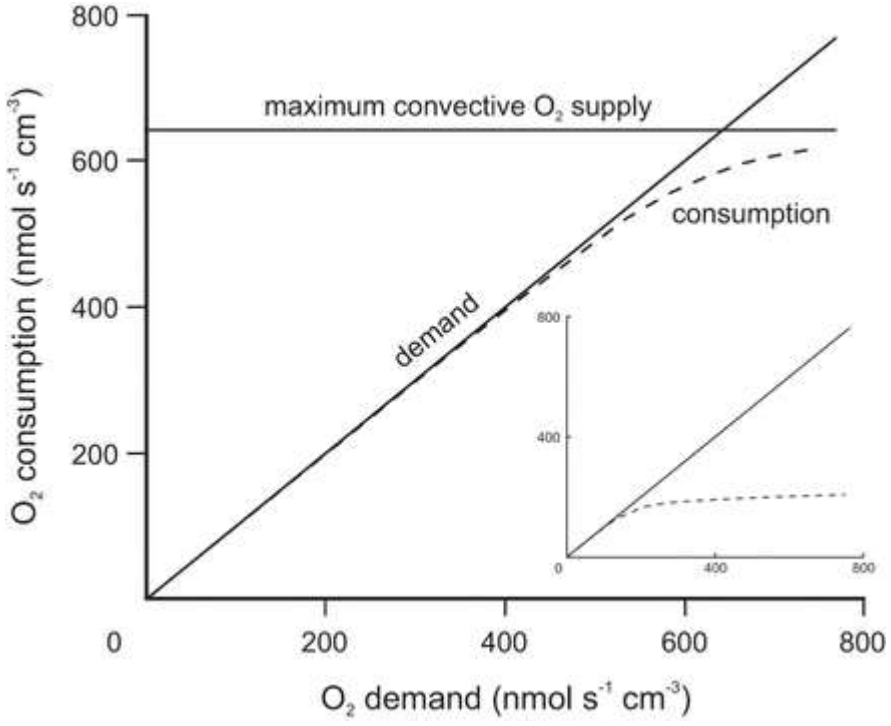

Fig. 3. Output of the oxygen transport model that we applied to the left ventricular tissue of sheep and goats showing the relationship between oxygen supply, demand, and consumption. Predicted oxygen consumption rate (nmol $O_2 \cdot s^{-1} \cdot cm^{-3}$ of tissue) keeps pace with an increasing oxygen demand rate (nmol $O_2 \cdot s^{-1} \cdot cm^{-3}$), except at very high levels of demand, where consumption is limited by the oxygen supply rate (nmol $O_2 \cdot s^{-1} \cdot cm^{-3}$). This is for the standard case assuming an external mechanical efficiency of 20%. *Inset*: same model as applied to skeletal muscle (47).

DISCUSSION

Our measurements of the body mass-specific left ventricular work rate of resting sheep and goats under mild sedation (0.029 W/kg) are comparable with previous estimates in these animals (~0.035 W/kg), calculated from published hemodynamic data (32, 33). The overall volume-specific left ventricular work rate of resting sheep and goats of 0.017 W/cm^3 of tissue equates to a volume-specific oxygen demand rate of 195 nmol $O_2 \cdot s^{-1} \cdot cm^{-3}$, and since oxygen supply is normally not limiting under resting conditions, oxygen consumption is predicted to match oxygen demand. However, during heavy exercise, oxygen demand by the left ventricular tissue is projected to increase by ~3.5-fold to ~670 nmol $O_2 \cdot s^{-1} \cdot cm^{-3}$. To test whether oxygen supply can satisfy demand during heavy exercise, we applied this augmented level of oxygen demand together with the dimensions of the left ventricle's capillary-tissue network to a three-dimensional oxygen transport model. The results of this model suggest that when oxygen demand is increased during heavy exercise, oxygen supply is just adequate to maintain Po_2 levels along the length of the cardiac capillary to drive oxygen into the surrounding tissue. At an oxygen demand rate of 670 nmol $O_2 \cdot s^{-1} \cdot cm^{-3}$ and an external mechanical efficiency of 20%, almost all cardiac tissue remains oxygenated, with only 9% of tissue operating at a Po_2 below the estimated p_{50cyt} of 0.05 kPa and only 1.8% operating below 0.01 kPa (Fig. 2*A*). A sensitivity test on the effect of varying the left ventricle's oxygen demand rate during heavy exercise shows that no tissue would have Po_2 < 0.01 kPa at oxygen demand rates <610 nmol $O_2 \cdot s^{-1} \cdot cm^{-3}$ but that approximately one-tenth of tissue would have Po_2 < 0.01 kPa at an oxygen demand rate of 810 nmol $O_2 \cdot s^{-1} \cdot cm^{-3}$ (Fig. 2*B*). A second sensitivity test, run over the typically reported range of external mechanical efficiencies of 15–25% (37, 61, 76), showed that no tissue would have Po_2 < 0.01 kPa at an efficiency above 22%, but that approximately one-tenth of tissue would have Po_2 < 0.01 kPa at an efficiency of 16% (Fig. 2*C*). To some extent, this small region of hypoxia is likely reduced by the longitudinal diffusion of oxygen in the tissue and by the convective mixing of oxygen in the tissue (19). Application of oxygen transport models incorporating time-dependent blood supply (e.g., 40, 54, 62) should also help deduce the temporal variation and relative extent of this small region of hypoxia and should be especially useful in the present context where higher blood flow rates occur during diastole than during systole (57).

Another important finding of the oxygen transport model is that during heavy exercise, the literature-derived oxygen supply rate, 645 nmol $O_2 \cdot s^{-1} \cdot cm^{-3}$ of tissue, appears to be well matched to oxygen demand rate, 670 nmol $O_2 \cdot s^{-1} \cdot cm^{-3}$, which allows oxygen consumption by the cardiac tissue to reach at least ~600 nmol $O_2 \cdot s^{-1} \cdot cm^{-3}$ or 90% of demand. This balance is in contrast to the situation in skeletal muscle, in which oxygen supply cannot keep pace with demand as it increases to its maximum rate during heavy exercise (Fig. 3) (47). The stark difference in the oxygen supply capacity of cardiac tissue compared with skeletal muscle can be traced to the approximately fivefold difference in the number of capillaries per cross-sectional area of fiber, which we found to be 3,151 mm^{-2} for the left ventricle vs. 400–800 mm^{-2} for skeletal muscle (30). This high cardiac capillary density facilitates oxygen supply by providing a larger endothelial surface area for oxygen transfer to the surrounding cardiomyocytes and by reducing the Krogh tissue cylinder radius (R_t), which reduces both the oxygen diffusion resistance and the mean volume of tissue serviced by each capillary. It is this capillary morphology that allows cardiac tissue metabolism to remain nearly entirely aerobic even during periods of heavy exercise, whereas skeletal muscle supports ~50% of its maximum work anaerobically (64).

Having established that the demand for oxygen by the left ventricular tissue is met under both resting conditions and during heavy exercise, we examined the mitochondria, which consume the oxygen in the process of generating ATP via oxidative phosphorylation. The enzymes involved in aerobic ATP synthesis are embedded in the inner mitochondrial

membrane, and so the surface density of this membrane provides an index of the mitochondria's oxidative capacity (28). The inner mitochondrial membrane surface density averaged across our sheep and goats was 37 m^2/cm^3 of mitochondria, which falls well within the range of 31–46 m^2/cm^3 reported for mitochondria in the left ventricle of mouse, cat, and cattle (25) and also aligns well with values of ~35 m^2/cm^3 reported for skeletal muscle in cat (63), dik-dik, and wildebeest (26). Because the inner mitochondrial membrane surface density of cardiac tissue is similar to that found in different skeletal muscle types (28, 75), the mitochondrial volume density can be used to infer the tissue's relative aerobic capacity. The volume density of mitochondria in the left ventricular cardiomyocytes of sheep and goats is 21–22%, which is at the lower end of the range (21–38%) previously reported for mammalian cardiac tissue (Fig. 4*A*). Nonetheless, the mitochondrial volume density of cardiac tissue is consistently greater than that reported for skeletal muscle, which typically falls within the range of 4–10% (23, 45). Prompted by this difference, we calculated the average oxygen consumption rate per unit volume of mitochondria in the cardiac tissue of sheep and goats under resting conditions and found it to be 1,150 nmol $O_2 \cdot s^{-1} \cdot cm^{-3}$ of mitochondria. Under conditions of heavy exercise the value increases to ~3,600 nmol $O_2 \cdot s^{-1} \cdot cm^{-3}$, which is close to the maximum value calculated for skeletal muscle mitochondria of 3,700 nmol $O_2 \cdot s^{-1} \cdot cm^{-3}$ (24). Thus cardiac and skeletal muscle mitochondria have similar in vivo functional capacities. Furthermore, our in vivo respiration rate for cardiac mitochondria during heavy exercise is within 80% of the maximum in vitro estimate of 4,300 nmol $O_2 \cdot s^{-1} \cdot cm^{-3}$ of mitochondria (63), which suggests that cardiac mitochondria operate close to their functional limits during heavy exercise.

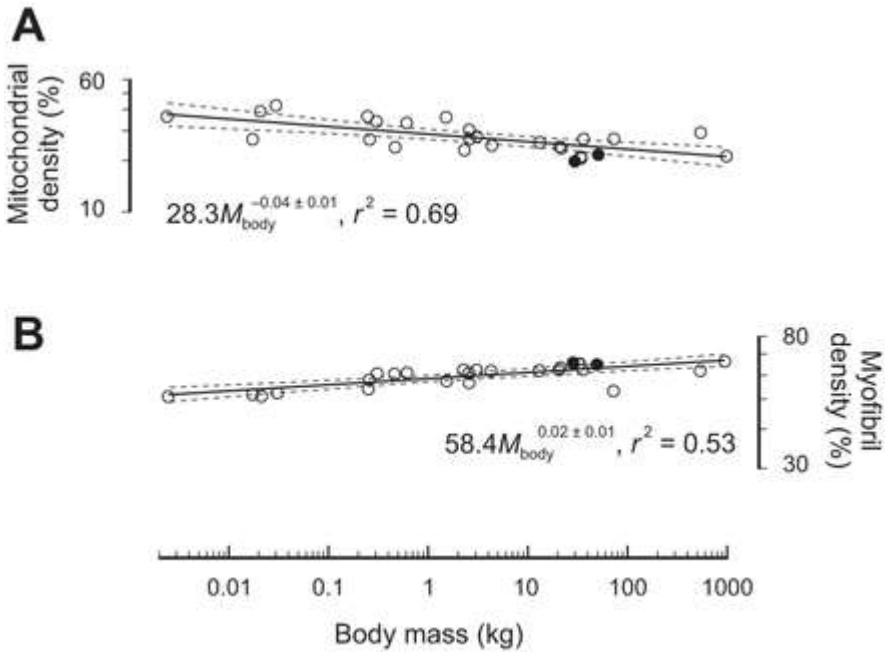

Fig. 4. Interspecific scaling of mitochondrial and myofibril volume density in the left ventricle of mammals. *A*: mitochondrial volume density (% of cardiomyocyte) in sheep and goats from the present study (●) and in other mammals sourced from the literature, including shrew, bat, wood mouse, house mouse, rat, guinea pig, ferret, rabbit, cat, fox, coyote, wolf, dog, goat, human, pig, horse, and cow (○) (5, 25, 36). *B*: myofibril volume density (% of cardiomyocyte) in sheep and goats from the present study and in the other mammals sourced from the literature. Myofibril volume densities in the other mammals are either published values or calculated by subtraction of the volume density of the mitochondria and of the other cardiomyocyte components (assumed to represent 12.7% of cardiomyocyte volume as determined in the present study). M_{body} is body mass (kg). Exponents are presented with ±95% CI.

The majority of ATP generated by the mitochondria is ultimately used by the myofibril contractile apparatus in the process of developing tension (= stress; force/area). Tension development is the defining role of muscle systems, and maximum tension is proportional to

the fraction of tissue occupied by the myofibrils (43). The volume density of myofibrils in the left ventricular cardiomyocytes of sheep and goats is 65–66%, which is at the upper end of the range (51–66%) calculated for a variety of mammalian species (Fig. 4*B*). The generation of tension by the myofibrils of the left ventricle is critical to cardiac function because it pressurizes the blood, allowing it to eject against the resistance of the systemic vascular circuit. According to the principle of Laplace, the pressure imparted to the blood also depends on left ventricular wall thickness and radius of curvature, which is expressed by the wall-to-lumen volume ratio. Tension acting in the direction of the fiber (σ_f; kPa) thus can be calculated according to the volume-averaged fiber stress model, $\sigma_f = P_b \cdot [(1/3)\ln(1 + V_{lv}/V_l)]^{-1}$, where P_b is the systemic arterial blood pressure (kPa) and V_{lv} and V_l are the left ventricular wall and lumen volume (cm^3), respectively (2). By applying sheep and goat systemic arterial diastolic blood pressure, left ventricular wall volume, and left ventricular end-diastolic lumen volume, as estimated from stroke volume and a 75% ejection fraction (21), we find that peak fiber tension averaged 55 kPa in our resting animals, and we predict it to increase to ~65 kPa during heavy exercise. These levels of peak fiber tension in the end-diastolic left ventricular wall are lower than active isometric tension (120–140 kPa) generated by isolated cardiac tissue (4, 55, 71) at realistic end-diastolic sarcomere lengths between 2.2 and 2.3 μm (65). This reserve capacity for tension development is evidently recruited by the left ventricle during isovolumetric contraction under an aortic clamp, which, although not a natural condition, does demonstrate an approximate twofold increase in peak blood pressure and fiber tension compared with isovolumetric contraction by the unclamped left ventricle at the same end-diastolic dimensions (1, 3). Thus, as shown for skeletal muscle (53), the left ventricle normally operates with some reserve capacity (~2-fold) for tension development, possibly providing a safety factor to protect cardiac tissue from high force loads during health while allowing for compensation of cardiac output and blood pressure during disease.

In summary, we undertook a structure-function analysis of the left ventricle at rest and during simulated heavy exercise, using sheep and goats as experimental models. Oxygen demand by the left ventricular cardiac tissue is modest in our resting animals, and so we calculated a 3.5-fold increase in demand to simulate heavy exercise and found that under these conditions, oxygen supply across the cardiac capillary network is just sufficient to maintain tissue Po_2 above that required to support aerobic metabolism. Thus oxygen consumption by the left ventricular mitochondria increases by approximately threefold from rest to heavy exercise, reaching within 80% of maximum in vitro rates, suggesting that cardiac mitochondria function close to their limits during heavy exercise. Finally, peak fiber tension generated by the myofibrils in the wall of the left ventricle is ~50% of maximum tensions recorded from isolated cardiac tissue and is explained by an apparent reserve capacity for tension development built into the left ventricle. With cardiovascular disease remaining the leading cause of death worldwide, structure-function analyses of the healthy and pathological states should complement future research efforts.

GRANTS

This research was supported by an Australian Research Council Discovery Project Award to R. S. Seymour, S. K. Maloney, and A. P. Farrell (DP-120102081). E. P. Snelling holds a South African Claude Leon Foundation Postdoctoral Fellowship. J. E. F. Green is supported by an Australian Research Council Discovery Early Career Researcher Award (DE-130100031). A. P. Farrell holds a Canada Research Chair and is supported by a Discovery Grant from the Natural Sciences and Engineering Research Council of Canada.

DISCLOSURES

No conflicts of interest, financial or otherwise, are declared by the author(s).

AUTHOR CONTRIBUTIONS

E.P.S., R.S.S., L.C.R.M., A.F., A.H., D.M., A.P.F., M.-A.C., and S.K.M. conception and design of research; E.P.S., L.C.R.M., A.F., A.H., D.M., M.-A.C., M.B., and S.K.M. performed experiments; E.P.S., R.S.S., J.E.F.G., and A.I. analyzed data; E.P.S., R.S.S., J.E.F.G., L.C.R.M., A.F., A.H., D.M., A.P.F., M.-A.C., A.I., M.B., and S.K.M. interpreted results of experiments; E.P.S. and J.E.F.G. prepared figures; E.P.S., R.S.S., J.E.F.G., L.C.R.M., A.F., A.H., D.M., A.P.F., M.-A.C., A.I., M.B., and S.K.M. drafted manuscript; E.P.S., R.S.S., J.E.F.G., L.C.R.M., A.H., D.M., A.P.F., M.-A.C., A.I., M.B., and S.K.M. edited and revised manuscript; E.P.S., R.S.S., J.E.F.G., L.C.R.M., A.F., A.H., D.M., A.P.F., M.-A.C., A.I., M.B., and S.K.M. approved final version of manuscript.

ACKNOWLEDGMENTS

The authors acknowledge the expertise and contribution made by the academics, technicians, and volunteers of the School of Physiology, and the Central Animal Service, at the University of the Witwatersrand. We especially thank David Gray, Gavin Norton, Angela Woodiwiss, and Zipho Zwane, Robyn Hetem, Benjamin Rey, Nico Douths, Peter Kamerman, Richard McFarland, Hilary Lease, Peter Buss, Michelle Miller, Tapiwa Chinaka, and W. Maartin Strauss.

REFERENCES

1. Arts T, Bovendeerd P, Delhaas T, Prinzen F. Modeling the relation between cardiac pump function and myofiber mechanics. *J Biomech* 36: 731–736, 2003.

2. Arts T, Bovendeerd PHM, Prinzen FW, Reneman RS. Relation between left ventricular cavity pressure and volume and systolic fiber stress and strain in the wall. *Biophys J* 59: 93–102, 1991.

3. Arts T, Reneman RS. *Conversion of fiber stress to global left ventricular pump work. In: Activation, Metabolism, and Perfusion of the Heart*, edited by Sideman S. Dordrecht, The Netherlands: Martinus Nijhoff, 1987, p. 353–364.

4. Backx PH, Gao WD, Azan-Backx MD, Marban E. The relationship between contractile force and intracellular [Ca^{2+}] in intact rat cardiac trabeculae. *J Gen Physiol* 105: 1–19, 1995.

5. Barth E, Stämmler G, Speiser B, Schaper J. Ultrastructural quantitation of mitochondria and myofilaments in cardiac muscle from 10 different animal species including man. *J Mol Cell Cardiol* 24: 669–681, 1992.

6. Bassingthwaighte JB, Yipintsoi T, Harvey RB. Microvasculature of the dog left ventricular myocardium. *Microvasc Res* 7: 229–249, 1974.

7. Batra S, Rakusan K. Capillary length, tortuosity, and spacing in rat myocardium during cardiac cycle. *Am J Physiol Heart Circ Physiol* 263: H1369–H1376, 1992.

8. Batra S, Rakusan K. Geometry of capillary networks in volume overloaded rat heart. *Microvasc Res* 42: 39–50, 1991.

9. Batra S, Rakusan K, Campbell SE. Geometry of capillary networks in hypertrophied rat heart. *Microvasc Res* 41: 29–40, 1991.

10. Bell AW, Hales JRS, King RB, Fawcett AA. Influence of heat stress on exercise-induced changes in regional blood flow in sheep. *J Appl Physiol* 55: 1916–1923, 1983.

11. Burton AC. *Physiology and Biophysics of the Circulation*. Chicago, IL: Year Book Medical, 1965.

12. Conley KE, Kayar SR, Rosler K, Hoppeler H, Weibel ER, Taylor CR. Adaptive variation in the mammalian respiratory system in relation to energetic demand: IV. Capillaries and their relationship to oxidative capacity. *Respir Physio*l 69: 47–64, 1987.

13. Cruz-Orive LM, Weibel ER. Recent stereological methods for cell biology: a brief survey. Am *J Physiol Lung Cell Mol Physiol* 258: L148–L156, 1990.

14. Dijkhuizen P, Buursma A, Fongers TME, Gerding AM, Oeseburg B, Zijlstra WG. The oxygen binding capacity of human haemoglobin: Hüfner's factor redetermined. *Pflugers Arch* 369: 223–231, 1977.

15. Duncker DJ, Bache RJ. Regulation of coronary blood flow during exercise. *Physiol Rev* 88: 1009–1086, 2008.

16. Egginton S. Morphometric analysis of tissue capillary supply. In: *Advances in Comparative and Environmental Physiology*, edited by Boutilier RG. Berlin: Springer-Verlag, 1990, vol. 6, p. 73–141.

17. Egginton S, Gaffney E. Tissue capillary supply: it's quality not quantity that counts! *Exp Physiol* 95: 971–979, 2010.

18. Folkow B, Neil E. *Circulation*. New York: Oxford University Press, 1971.

19. Goldman D. Theoretical models of microvascular oxygen transport to tissue. *Microcirculation* 15: 795–811, 2008.

20. Gros G, Wittenberg BA, Jue T. Myoglobin's old and new clothes: from molecular structure to function in living cells. *J Exp Biol* 213: 2713–2725, 2010.

21. Hallowell GD, Potter TJ, Bowen IM. Reliability of quantitative echocardiography in adult sheep and goats. *BMC Vet Res* 8: 181, 2012.

22. Hellums JD, Nair PK, Huang NS, Ohshima N. Simulation of intraluminal gas transport processes in the microcirculation. *Ann Biomed Eng* 24: 1–24, 1996.

23. Hoppeler H, Kayar SR, Claassen H, Uhlmann E, Karas RH. Adaptive variation in the mammalian respiratory system in relation to energetic demand: III. Skeletal muscles: setting the demand for oxygen. *Respir Physiol* 69: 27–46, 1987.

24. Hoppeler H, Lindstedt SL. Malleability of skeletal muscle in overcoming limitations: structural elements. *J Exp Biol* 115: 355–364, 1985.

25. Hoppeler H, Lindstedt SL, Claassen H, Taylor CR, Mathieu O, Weibel ER. Scaling mitochondrial volume in heart to body mass. *Respir Physiol* 55: 131–137, 1984.

26. Hoppeler H, Mathieu O, Krauer R, Claassen H, Armstrong RB,Weibel ER. Design of the mammalian respiratory system: VI. Distribution of mitochondria and capillaries in various muscles. *Respir Physiol* 44: 87–111, 1981.

27. Hoppeler H, Mathieu O, Weibel ER, Krauer R, Lindstedt SL, Taylor CR. Design of the mammalian respiratory system: VIII. Capillaries in skeletal muscles. *Respir Physiol* 44: 129–150, 1981.

28. Hoppeler H, Weibel ER. Structural and functional limits for oxygen supply to muscle. *Acta Physiol Scand* 168: 445–456, 2000.

29. Howard CV, Reed MG. *Unbiased Stereology: Three Dimensional Measurement in Microscopy*. Oxford: BIOS Scientific, 1998.

30. Hudlicka O, Brown M, Egginton S. Angiogenesis in skeletal and cardiac muscle. *Physiol Rev* 72: 369–417, 1992.

31. Jones JH, Longworth KE, Lindholm A, Conley KE, Karas RH, Kayar SR, Taylor CR. Oxygen transport during exercise in large mammals: I. Adaptive variation in oxygen demand. *J Appl Physiol* 67: 862–870, 1989.

32. Kane DW, Tesauro T, Newman JH. Adrenergic modulation of the pulmonary circulation during strenuous exercise in sheep. *Am Rev Respir* Dis 147: 1233–1238, 1993.

33. Karas RH, Taylor CR, Rösler K, Hoppeler H. Adaptive variation in the mammalian respiratory system in relation to energetic demand: V. Limits to oxygen transport by the circulation. *Respir Physiol* 69: 65–79, 1987.

34. Kassab GS, Fung YCB. Topology and dimensions of pig coronary capillary network. *Am J Physiol Heart Circ Physiol* 267: H319–H325, 1994.

35. Keen EN. The postnatal development of the human cardiac ventricles. *J Anat* 89: 485–502, 1955.

36. Kim HD, Kim CH, Rah BJ, Chung HI, Shim TS. Quantitative study on the relation between structural and functional properties of the hearts from three different mammals. *Anat Rec* 238: 199–206, 1994.

37. Knaapen P, Germans T, Knuuti J, Paulus WJ, Dijkmans PA, Allaart CP, Lammertsma AA, Visser FC. Myocardial energetics and efficiency: Current status of the noninvasive approach. *Circulation* 115: 918–927, 2007.

38. Kreuzer F. Oxygen supply to tissues: The Krogh model and its assumptions. *Experientia* 38: 1415–1426, 1982.

39. Krogh A. The number and distribution of capillaries in muscles with calculations of the oxygen pressure head necessary for supplying the tissue. *J Physiol* 52: 409–415, 1919.

40. Lagerlund TD, Low PA. Mathematical modeling of time-dependent oxygen transport in rat peripheral nerve. *Comput Biol Med* 23: 29–47, 1993.

41. Lahiri S. Blood oxygen affinity and alveolar ventilation in relation in body weight in mammals. *Am J Physiol* 229: 529–536, 1975.

42. Lin PC, Kreutzer U, Jue T. Myoglobin translational diffusion in rat myocardium and its implication on intracellular oxygen transport. *J Physiol* 578: 595–603, 2007.

43. Lindstedt SL, McGlothlin T, Percy E, Pifer J. Task-specific design of skeletal muscle: Balancing muscle structural composition. *Comp Biochem Physiol Part B Biochem Mol Biol* 120: 35–40, 1998.

44. Mathieu-Costello O. Comparative aspects of muscle capillary supply. *Annu Rev Physiol* 55: 503–525, 1993.

45. Mathieu O, Krauer R, Hoppeler H, Gehr P, Lindstedt SL, Alexander RM, Taylor CR, Weibel ER. Design of the mammalian respiratory system: VII. Scaling mitochondrial volume in skeletal muscle to body mass. *Respir Physiol* 44: 113–128, 1981.

46. Mayhew TM. The new stereological methods for interpreting functional morphology from slices of cells and organs. *Exp Physiol* 76: 639–665, 1991.

47. McGuire BJ, Secomb TW. A theoretical model for oxygen transport in skeletal muscle under conditions of high oxygen demand. *J Appl Physiol* 91: 2255–2265, 2001.

48. ühlfeld C, Nyengaard JR, Mayhew TM. A review of state-of-the-art stereology for better quantitative 3D morphology in cardiac research. *Cardiovasc Pathol* 19: 65–82, 2010.

49. Mundie TG, Januszkiewicz AJ, Ripple GR. Effects of epinephrine, phenoxybenzamine, and propranolol on maximal exercise in sheep. *Lab Anim Sci* 42: 486–490, 1992.

50. O'Brien PJ, Shen H, McCutcheon LJ, O'Grady M, Byrne PJ, Ferguson HW, Mirsalimi S, Julian RJ, Sargeant JM, Tremblay RRM, Blackwell TE. Rapid, simple and sensitive microassay for skeletal and cardiac muscle myoglobin and hemoglobin: Use in various animals indicates functional role of myohemoproteins. *Mol Cell Biochem* 112: 45–52, 1992.

51. Opie LH. *The Heart: Physiology, From Cell to Circulation* (3rd ed.). Philadelphia, PA: Lippincott-Raven, 1998.

52. Papadopoulos S, Endeward V, Revesz-Walker B, Jürgens KD, Gros G. Radial and longitudinal diffusion of myoglobin in single living heart and skeletal muscle cells. *Proc Natl Acad Sci U S A* 98: 5904–5909, 2001.

53. Perry AK, Blickhan R, Biewener AA, Heglund NC, Taylor CR. Preferred speeds in terrestrial vertebrates: are they equivalent? *J Exp Biol* 137: 207–219, 1988.

54. Piiper J, Scheid P. Diffusion limitation of O_2 supply to tissue in homogeneous and heterogeneous models. *Respir Physiol* 85: 127–136, 1991.

55. Pollack GH, Krueger JW. Sarcomere dynamics in intact cardiac muscle. *Eur J Cardiol* 4, Suppl: 53–65, 1976.

56. Popel AS. Theory of oxygen transport to tissue. *Crit Rev Biomed Eng* 17: 257–321, 1989.

57. Recchia FA, Senzaki H, Saeki A, Byrne BJ, Kass DA. Pulse pressure-related changes in coronary flow in vivo are modulated by nitric oxide and adenosine. *Circ Res* 79: 849–856, 1996.

58. Richmond KN, Burnite S, Lynch RM. Oxygen sensitivity of mitochondrial metabolic state in isolated skeletal and cardiac myocytes. *Am J Physiol Cell Physiol* 273: C1613–C1622, 1997.

59. Rossi-Fanelli A, Antonini E. Studies on the oxygen and carbon monoxide equilibria of human myoglobin. *Arch Biochem Biophys* 77: 478–492, 1958.

60. Schenkman KA, Marble DR, Burns DH, Feigl EO. Myoglobin oxygen dissociation by multiwavelength spectroscopy. *J Appl Physiol* 82: 86–92, 1997.

61. Schipke JD. Cardiac efficiency. *Basic Res Cardiol* 89: 207–240, 1994.

62. Schumacker PT, Samsel RW. Analysis of oxygen delivery and uptake relationships in the Krogh tissue model. *J Appl Physiol* 67: 1234–1244, 1989.

63. Schwerzmann K, Hoppeler H, Kayar SR, Weibel ER. Oxidative capacity of muscle and mitochondria: correlation of physiological, biochemical, and morphometric characteristics. *Proc Natl Acad Sci U S A* 86: 1583–1587, 1989.

64. Seymour RS. Maximal aerobic and anaerobic power generation in large crocodiles versus mammals: implications for dinosaur gigantothermy. *PLoS One* 8: e69361, 2013.

65. Shiels HA, White E. The Frank-Starling mechanism in vertebrate cardiac myocytes. *J Exp Biol* 211: 2005–2013, 2008.

66. Stanley WC, Recchia FA, Lopaschuk GD. Myocardial substrate metabolism in the normal and failing heart. *Physiol Rev* 85: 1093–1129, 2005.

67. Stegmann GF, Bester L. Sedative-hypnotic effects of midazolam in goats after intravenous and intramuscular administration. *Vet Anaesth Analg* 28: 49–55, 2001.

68. Sugawara J, Tanabe T, Miyachi M, Yamamoto K, Takahashi K, Iemitsu M, Otsuki T, Homma S, Maeda S, Ajisaka R, Matsuda M. Non-invasive assessment of cardiac output during exercise in healthy young humans: comparison between Modelflow method and Doppler echocardiography method. *Acta Physiol Scand* 179: 361–366, 2003.

69. Swenson ER. Kinetics of oxygen and carbon dioxide exchange. In: *Advances in Comparative and Environmental Physiology*, edited by Boutilier RG. Berlin: Springer-Verlag, 1990, vol. 6, p. 163–210.

70. Taylor CR, Karas RH, Weibel ER, Hoppeler H. Adaptive variation in the mammalian respiratory system in relation to energetic demand: II. Reaching the limits to oxygen flow. *Respir Physiol* 69: 7–26, 1987.

71. ter Keurs HEDJ, Rijnsburger WH, van Heuningen R, Nagelsmit MJ. Tension development and sarcomere length in rat cardiac trabeculae: evidence of length-dependent activation. *Circ Res* 46: 703–714, 1980.

72. van der Laarse WJ, des Tombe AL, van Beek-Harmsen BJ, Lee-de Groot MBE, Jaspers RT. Krogh's diffusion coefficient for oxygen in isolated Xenopus skeletal muscle fibers and rat myocardial trabeculae at maximum rates of oxygen consumption. *J Appl Physiol* 99: 2173–2180, 2005.

73. Vinnakota KC, Bassingthwaighte JB. Myocardial density and composition: a basis for calculating intracellular metabolite concentrations. *Am J Physiol Heart Circ Physiol* 286: H1742–H1749, 2004.

74. Weibel ER, Hoppeler H. Exercise-induced maximal metabolic rate scales with muscle aerobic capacity. *J Exp Biol* 208: 1635–1644, 2005.

75. Weibel ER, Taylor CR, Hoppeler H. The concept of symmorphosis: a testable hypothesis of structure-function relationship. *Proc Natl Acad Sci U S A* 88: 10357–10361, 1991.

76. Westerhof N. Cardiac work and efficiency. *Cardiovasc Res* 48: 4–7, 2000.

77. Wilson DF, Rumsey WL, Green TJ, Vanderkooi JM. The oxygen dependence of mitochondrial oxidative phosphorylation measured by a new optical method for measuring oxygen concentration. *J Biol Chem* 263: 2712–2718, 1988.

78. Zar JH. *Biostatistical Analysis*. Upper Saddle River, NJ: Prentice Hall, 1998.